Research article

Hao Jiang, Changbin Nie, Jintao Fu, Linlong Tang, Jun Shen, Feiying Sun, Jiuxun Sun*, Meng zhu, Shuanglong Feng, Yang Liu, Haofei Shi* and Xingzhan Wei*

Ultrasensitive and fast photoresponse in graphene/silicon-on-insulator hybrid structure by manipulating the photogating effect

https://doi.org/10.1515/nanoph-2020-0261
Received April 29, 2020; accepted June 4, 2020; published online June 29, 2020

Abstract: The hybrid structures of graphene with semiconductor materials based on photogating effect have attracted extensive interest in recent years due to the ultrahigh responsivity. However, the responsivity (or gain) was increased at the expense of response time. In this paper, we devise a mechanism which can obtain an enhanced responsivity and fast response time simultaneously by manipulating the photogating effect (MPE). This concept is demonstrated by using a graphene/silicon-on-insulator (GSOI) hybrid structure. An ultrahigh responsivity of more than 10^7 A/W and a fast response time of 90 μs were obtained. The specific detectivity D^* was measured to be 1.46×10^{13} Jones at a wavelength of 532 nm. The Silvaco TCAD modeling was carried out to explain the manipulation effect, which was further verified by the GSOI devices with different doping levels of graphene in the experiment. The proposed mechanism provides excellent guidance for modulating carrier distribution and transport, representing a new route to improve the performance of graphene/semiconductor hybrid photodetectors.

Keywords: graphene; manipulation; photodetector; photogating effect; silicon-on-insulator.

***Corresponding authors: Jiuxun Sun**, School of Physics, University of Electronic Science and Technology of China, Chengdu, 610054, China, E-mail: sjx@uestc.edu.cn; **Haofei Shi**, Chongqing Institute of Green and Intelligent Technology, Chinese Academy of Sciences, Chongqing, 400714, China, E-mail: shi@cigit.ac.cn; and **Xingzhan Wei**, Chongqing Institute of Green and Intelligent Technology, Chinese Academy of Sciences, Chongqing, 400714, China, E-mail: weixingzhan@cigit.ac.cn
Hao Jiang: School of Physics, University of Electronic Science and Technology of China, Chengdu, 610054, China; Chongqing Institute of Green and Intelligent Technology, Chinese Academy of Sciences, Chongqing, 400714, China
Changbin Nie, Jintao Fu, Linlong Tang, Jun Shen, Feiying Sun and Shuanglong Feng: Chongqing Institute of Green and Intelligent Technology, Chinese Academy of Sciences, Chongqing, 400714, China
Meng zhu: TianJin Jinhang Insitute of Technical Physics, Tianjin, 300192, China
Yang Liu: Department of Physics, Harbin Institute of Technology, Harbin, 150001, China

1 Introduction

Graphene is considered as a promising material for photodetectors because of its unique properties of extremely high carrier mobility and ultra-broadband photoresponse [1–6]. However, the low optical absorption and short carrier lifetime usually lead to a low photoelectric response for monolayer graphene devices [7]. Optical resonators [8, 9], metal gratings, and plasmonic nanostructures can promote the interaction between graphene and light [10–12], which improves the light responsivity to a certain degree. But, the problem of low responsivity cannot be thoroughly solved by such optical manipulation methods. Thus, the photogating mechanism [13] based on hybrid structures of graphene with other semiconductor materials, such as quantum dots [14, 15], perovskites [16], carbon nanotubes [17], and MoS_2 [18], has been shown to efficiently improve the responsivity. However, the responsivity was increased at the expense of response time, and the overall performance is still restricted by the photogating effect.

Effective control of electron coupling at the heterojunction interface has become a critical issue to improve the photogating effect [18–25]. One method is to introduce an electric field at the interface to control the Schottky barrier directly. However, slow response speeds are still caused by the long-lived trapping of charges, which are often manifested as hysteresis in gate-voltage sweeps [18–22], as observed in the Graphene–silicon photodetector [23] and graphene–CQD photodiode [24]. Therefore, it is imperative to develop a new mechanism and method to improve the sensitivity and response speed of photodetectors simultaneously.

In this work, a new mechanism called manipulating the photogating effect (MPE) is proposed, and which is validated by using the graphene/silicon-on-insulator (GSOI) hybrid photodetector in photoconductive mode. By the MPE mechanism, the enhanced built-in potential of heterojunction and carrier concentration gradient in silicon can be controllably manipulated to improve the sensitivity and response speed of the device simultaneously. The experimental results demonstrate that a high responsivity can be obtained without the sacrifice of responding bandwidth for the first time, namely, it does not slow down the photoresponse speed caused by the long-lived trapping of charges [18, 23]. The responsivity of the GSOI device by MPE can reach 10^7 A/W, which is 10 times higher than that without vertical voltage, and the response time can be shortened from 1000 μs to 90 μs. A detectivity (D^*) of 1.46×10^{13} Jones was measured, which is superior to the reported silicon/graphene hybrid photodetectors [1, 23, 25–30]. Besides, we analyzed the carrier distribution and coupling behavior of the graphene-silicon interface by using the Silvaco TCAD software. A model between the manipulation law of device and vertical voltage was established, which is consistent well with the experimental results. These results confirm the vital role of manipulation effects in optoelectronic conversion and pave the way to explore novel fast and high-responsivity photodetectors.

2 Results and discussion

The GSOI heterostructure photodetector is schematically shown in Figure 1A. The SOI wafers with lightly doped p-type silicon layers on top of a buried silicon oxide film were employed. A monolayer graphene as the conducting channel was transferred onto the top-silicon surface by wet transfer method. Au films were deposited onto the surface of graphene to form an Ohmic contact (see Figure S1 of Supplementary Material) using electron beam evaporation. Both the source and drain electrodes were patterned via a lift-off process. Subsequently, the graphene film was patterned into strips by bilayer photolithography and dry etching process (see details in the Methods section). Figure 1B shows the SEM image of the GSOI device, in which the surface morphology of graphene is extremely smooth to ensure excellent contact with the underlying silicon.

When light illuminates on the GSOI device, photogenerated electron-hole pairs are generated in the top-silicon and separated under the built-in potential at the junction of graphene and silicon. Graphene behaves as a fast transfer channel of photogenerated charge herein. In MPE mechanism, when a vertical voltage is applied, the accumulation of induced charge on the two sides of silicon oxide will be manipulated, which will change the carrier concentration in the top-silicon [31]. The excess electrons or holes will inject into graphene, resulting in a change of sheet current. The energy band diagrams of the photodetector under the positive and negative vertical voltage conditions are as shown in Figure 1C and D respectively. Because the top-silicon is extremely thin (220 nm), the concentration and distribution gradient of carriers in top-silicon can be readily influenced by the induced charges. The remarkable increment of holes or electrons in top-silicon will break the dynamic equilibrium of the heterojunction between the graphene and top-silicon, and greatly alters the Fermi level of graphene. It should be noted that the carrier concentration of graphene is about 10^{12} cm^{-2}, which is far less than the p-doped silicon (10^{17} cm^{-2}). Thus, the variation of graphene's Fermi level is more obvious than silicon that can be ignored [27]. By adjusting the concentration, an increased built-in potential is formed between graphene and top-silicon to improve the separation efficiency of photocarriers. Moreover, the concentration gradient formed by the accumulation of carriers will speed up the diffusion of photogenerated carriers to the heterojunction region. Therefore, both high gain and fast photoresponse can be achieved through the manipulation effect in GSOI heterostructure.

The effects of MPE on lightly p-doped graphene devices were firstly investigated. The bipolarity of such device was exploited [32, 33], and the doping level of graphene was obtained by measuring the transfer curves, as plotted in Figure S2. The relationship of I_{ds} with V_{ds} is shown in Figure 2A, which demonstrates that V_g has a crucial influence on the magnitude and slope of I_{ds}. When V_g is negative, the I_{ds} are relatively large. In contrast, the I_{ds} would become relatively small as V_g turns positive.

The GSOI photodetector was illuminated by a visible laser with 532 nm wavelength accompanied with one optical attenuator, to obtain an adjustable input power. Figure 2B shows the variation of I_{ds} with V_g under different light powers. As V_g varies from –60 to 60 V, all I_{ds} curves exhibit a similar trend, namely, the photocurrent dramatically decreases from a high value to an "inflection point" around 0 V, and gradually rises afterward as V_g further increases. Such phenomenon can be attributed to the carrier manipulation in the graphene. For the lightly p-doped graphene, the holes play a major role in the conductance of graphene when $V_g = 0$ V. When a negative V_g is applied, a number of holes accumulate in the top-silicon and inject into the adjacent graphene, thus the I_{ds} produces a noticeable

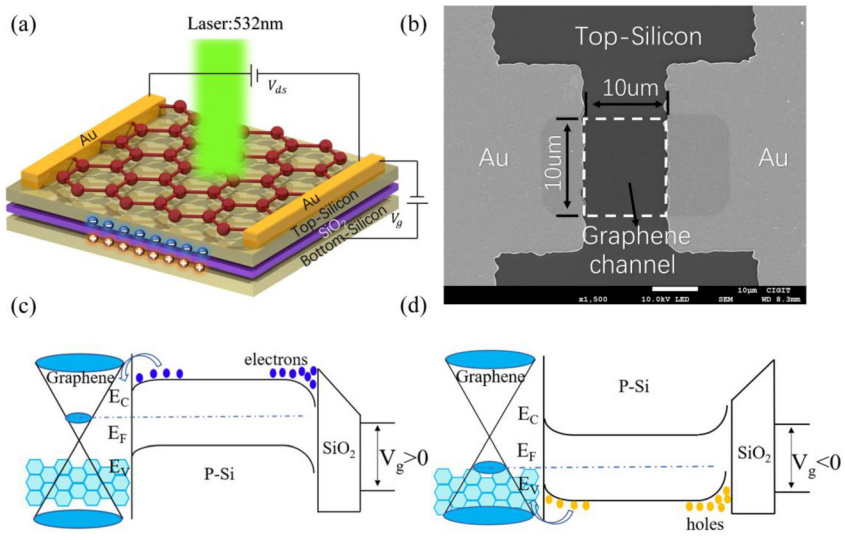

Figure 1: (a) Schematic view of the graphene/silicon-on-insulator (GSOI) heterojunction device in photoconductive mode. (b) SEM image of the GSOI device. The monolayer graphene strip (10 × 10 μm) directly attaches to the top-silicon, as shown in the dotted wireframe. (c) Energy band diagrams of the photodetector under positive vertical voltage. (d) Energy band diagrams of the photodetector under negative vertical voltage. Electrons and holes are denoted by blue and yellow circles, respectively.

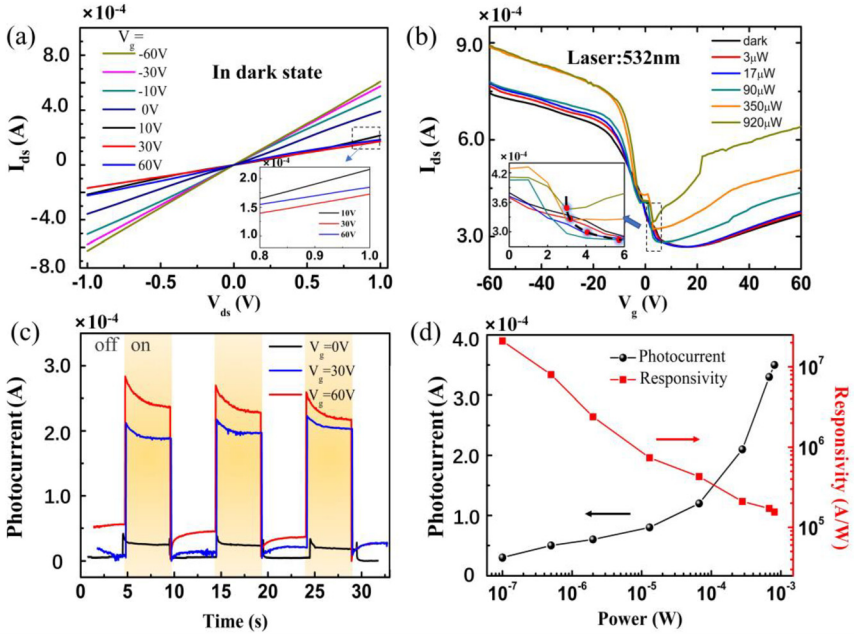

Figure 2: (a) Relationship of source-drain current (I_{ds}) with source-drain voltage (V_{ds}) under different V_g in the dark state. The inset shows the curve details of V_g = 10, 30, and 60 V. (b) I_{ds} as a function of the vertical voltage under different optical powers. The inset shows the curve details around the "inflection point". (c) Time-dependent photoresponse to the periodic chopping of the light source when V_g = 0, 30, and 60 V. The yellow and white region corresponds to the light-adding and non-light period, respectively. The illumination power is 920 μw. (d) Responsivity and photocurrent versus different optical power when V_g = 30 V.

increment. When V_g turns positive and is still smaller than the voltage of the "inflection point", the I_{ds} declines, because the graphene becomes doped by electrons instead of holes. As the further increase of V_g, abundant electrons will be injected into graphene, leading to a drastic increase of I_{ds}. In short, the "inflection point" corresponds to the transition of the type of majority carrier in graphene. Note that the "inflection point" makes a tiny shift with the increasing of optical power, as shown in the inset of Figure 2B. Because more carriers can be photogenerated and more electrons can be injected into graphene as the optical power increases, therefore, a relatively smaller V_g is required to induce the "inflection point".

Figure 2C shows the photocurrent response under different V_g as the laser light was chopped on and off, which shows an excellent reproducibility. Note that there is a dramatic enhancement when V_g changes from 0 to 60 V, which shows the vital effect of voltage manipulation. During the illumination, a trend that the photocurrent decreases with time can be observed. The rapid rise is assigned to the photo-generated electrons swept into graphene, whereas the following decreasement with slow

speed is ascribed to the hole injection into graphene during the diffusion process [27]. The photocurrent exhibits a gradual enhancement when the incident power ranges from 10^{-7} to 10^{-3} W, as shown in Figure 2D. The photocurrent can be up to 3×10^{-5} A when the intensity of light is 0.1 μW. In comparison, the photoresponse of SOI photodetector without graphene is shown in Figure S3, which shows that the introduction of graphene greatly improves the optoelectronic performance. The maximum responsivity of the GSOI device is calculated to be 2×10^{7} A/W, by using the formula $R = \frac{\Delta I}{P_e} = (I_{\text{light}} - I_{\text{dark}}) \times \left(P \times \frac{S_{\text{device}}}{S_{\text{light}}} \right)^{-1}$, where ΔI is photocurrent, P is optical power, S_{device} and S_{light} are the areas of active region and spot, respectively (See details in Table S1 of Supplementary Material). Note that this value is significantly larger than the reported graphene-silicon hybrid photodetector [23, 26–27], which can be ascribed to the manipulation effect reduced by the gate voltage in the GSOI device.

In order to systematically clarify the manipulation effect in such GSOI device, the modeling using Silvaco TCAD tools was carried out to compare with the experiment results. The basic parameters of graphene, such as bandgap, affinity, mobility, etc. were redefined by modifying the new material in database, through which the doping effect of graphene in the FET device has been fully proved [34, 35]. The modeling details are shown in Figure S4 of Supplementary Material. Figure 3A shows the experimental and modeled results about the relationship between I_{ds} and V_g in the dark state, which are in good agreement.

Figure 3B–D shows the distribution of majority carriers (holes) in top-silicon as V_g = 0, −30 and 30 V, respectively. When V_g = 0 V, the carrier distribution in silicon is only affected by the built-in potential and source-drain bias, as shown in Figure 3B. When V_g = −30 V, the induced holes would accumulate around the interface between the silicon dioxide and top-silicon, and the population of holes in top-silicon is larger than the case of V_g = 0 V, as shown in Figure 3C. Within a certain range, the distribution of holes will become denser as the negative vertical voltage increases. The non-equilibrium carriers generated in silicon will cause the injection of holes into graphene. Moreover, the Fermi energy level of graphene will alter more obviously than silicon [27]. The relevant energy band diagram is shown in the inset of Figure 3C, in which an enhanced built-in electric field is formed with the direction towards graphene. Under illumination, the photogenerated carriers

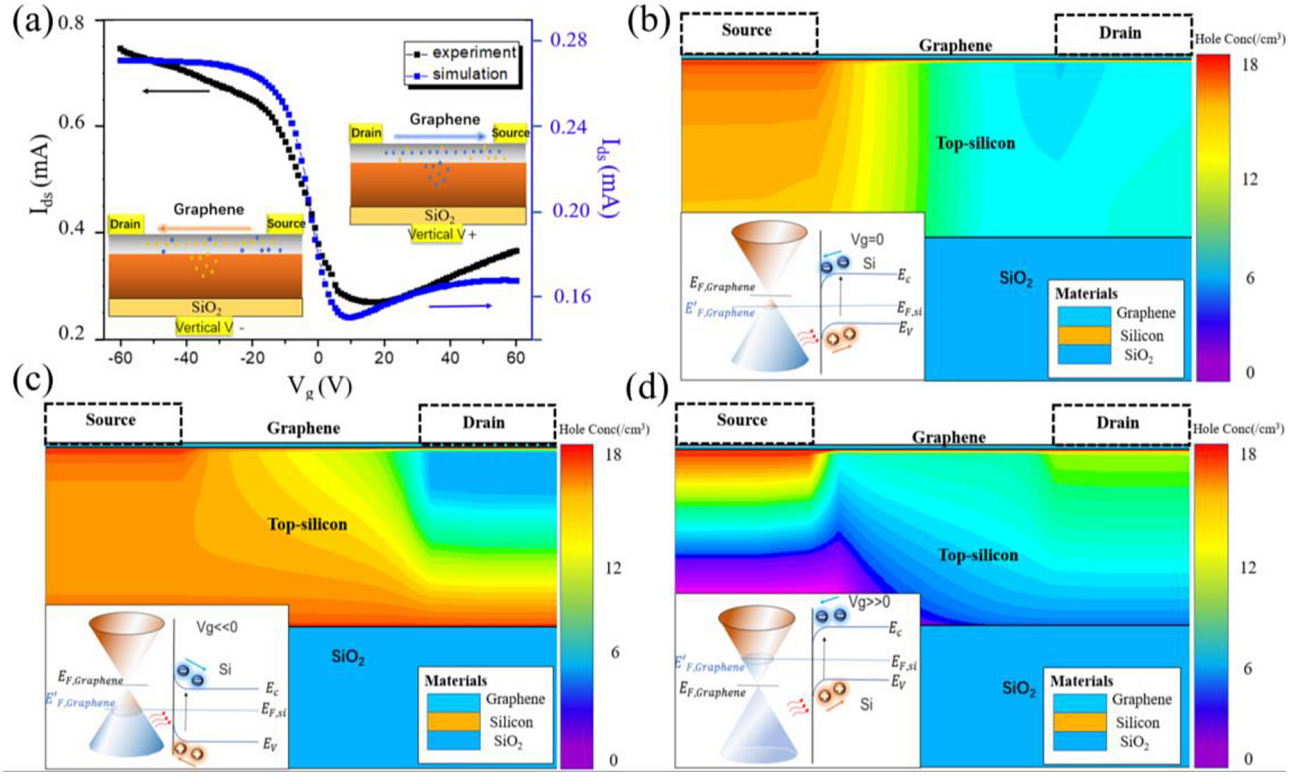

Figure 3: (a) Experimental (black line) and simulated (blue line) transfer characteristics in the dark state. The insets are the corresponding schematic views of the carrier transport under the positive and negative voltages. (b)–(d) Simulated holes distribution in silicon when V_g = 0, −30 and 30 V. Insets are the energy band diagrams.

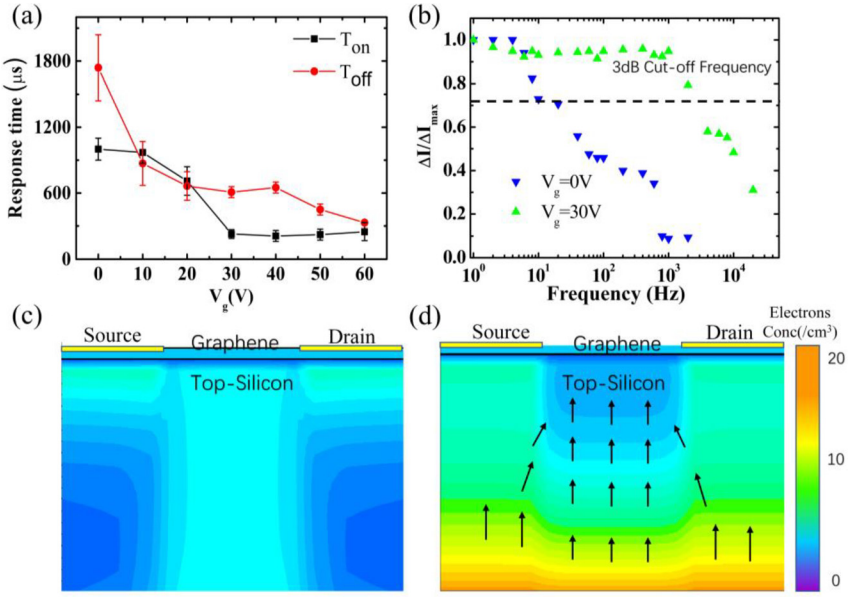

Figure 4: (a) Response time of the GSOI device versus the vertical voltage, error bars of T_{on} and T_{off} represent the rising and falling time, respectively. (b) 3 dB bandwidth measurement results of the GSOI device under 532 nm illumination when V_g = 0 V and V_g = 30 V, respectively. (c) Simulated distribution of electrons in top-silicon when V_g = 0 V. (d) Simulation concentration gradient formed by electrons in top-silicon when V_g = 30 V.

are separated into electrons and holes with the assistance of the enhanced built-in potential, and subsequently the holes will be injected into graphene, which gives rise to an increment of the photocurrent.

When V_g = 30 V, the induced electrons would accumulate around the interface of silicon dioxide and top-silicon, and the number of holes in top-silicon exhibits an obvious decrease comparing with the case V_g = 0 V, as shown in Figure 3D. As the vertical voltage increases, fewer holes (or more electrons) will distribute in top-silicon. This process changes the dynamic equilibrium between the heterojunction and leads to electron injection into graphene. Because the holes in graphene act as the majority carriers, the implantation of electrons into the graphene channel would reduce the source-drain current, which is consistent with the experimental results. With the further increase of the vertical voltage, a large number of electrons are injected into graphene, and the type of majority carrier changes to electrons. The source-drain current would exhibit an increment as the vertical voltage further increases. The Fermi level changes greatly, which is also much larger than the variation of Fermi level in silicon. An increased built-in electric field is formed pointing to top-silicon, which corresponds to the situation under positive vertical voltage in Figure 2B. The relevant energy band is shown in the inset of Figure 3D. Under illumination, electrons are injected into graphene, and the source-drain current would be greatly enhanced. More simulation results about current distribution are shown in Figure S5 of Supplementary Material.

This phenomenon can be explained by the change of resistance in the graphene channel [27, 36, 37].

$$R_{\text{modulation}} = R_{\text{contact}} + R_{\text{channel}} = R_{\text{contact}} + \frac{L/W}{(n+\Delta n)e\mu}, \quad (1)$$

$$E_F = E_{F\ \text{Dark}} + \Delta\Phi_{\text{bi}} = \hbar V_F \sqrt{\pi(n+\Delta n)} = 11.65\sqrt{(n+\Delta n)/(10^{10}\text{cm}^{-2})} \quad (2)$$

The $R_{\text{modulation}}$ represents the total resistance of the device, which consists of the contact resistance R_{contact} and the channel resistance R_{channel} under dark conditions, as expressed by formula (1). e is the elementary charge, W and L are the width and length of the channel, n and μ are the carrier concentration and carrier mobility, respectively, and Δn is the variation of carrier concentration generated by the voltage manipulation. The contact resistance is very small because there is Ohmic contact between graphene and the electrode. The resistance variation in the graphene channel is mainly dominated by Δn. The Fermi level of silicon nearly does not change under different gate voltages, therefore the variation of Schottky barrier height, $\Delta\Phi_{\text{bi}}$, is equivalent to the shift of graphene work function $\Delta\Phi_{\text{g}}$. Eventually, the Fermi energy of graphene can be expressed as $E_F = E_{F\ \text{Dark}} + \Delta\Phi_{\text{bi}}$ under different vertical voltages, as expressed by formula (2). Through the manipulation, a higher Schottky barrier height between graphene and top-silicon was formed, which leads to an increased built-in electric field and therefore improve the photocurrent [31].

Next, we discuss the effect of the MPE mechanism on the response time. The corresponding rising and falling times have been measured, as shown in Figure 4A, which can be greatly improved by increasing the vertical voltage. The rising time was reduced from 1 ms to about 100 μs, and

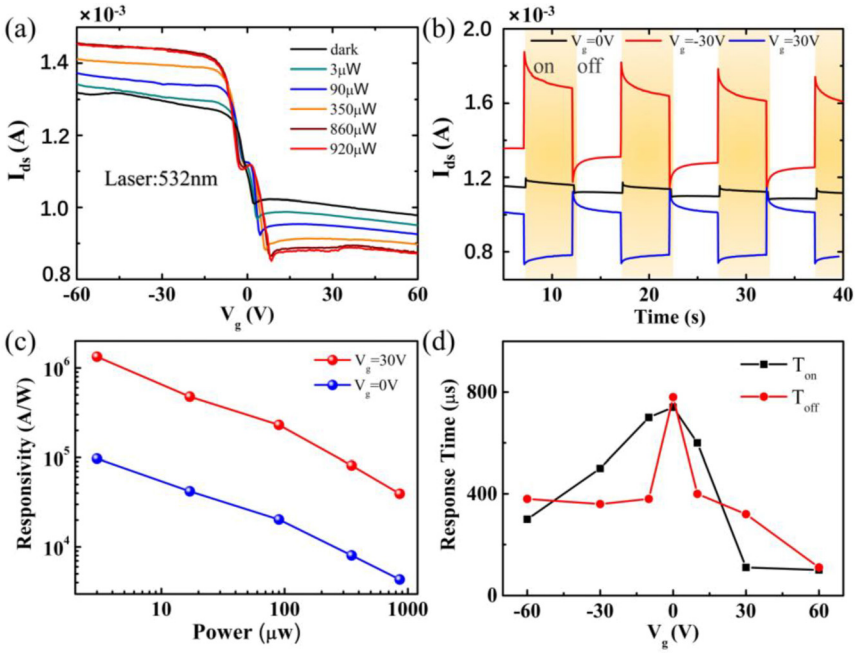

Figure 5: (a) I_{ds} as a function of V_g under 532 nm illumination light with different optical power. V_g increases from −60 to 60 V. (b) I_{ds}-Time curve of the device when V_g = 0 V, −30, and 30 V. (c) Responsivity versus light power when V_g = 30 and 0 V. (d) Response time at different vertical voltages.

the falling time was changed from 1.74 ms to about 200 μs, which are much faster than other reported photogating type devices [23]. Note that our GSOI device enables simultaneously high signal amplification and rapid response. Figure 4B shows the 3 dB bandwidth test results of the GSOI photodetector, in which we can find that the bandwidth is greatly improved when V_g = 30 V in comparison with the case of V_g = 0 V.

The process of carrier generation and diffusion in the heterojunction region has a great influence on the photoresponse [24]. The slow diffusion speed gives rise to a long response time. The carrier distribution when V_g = 0 V is shown in Figure 4C, and it can be found that there is nearly no concentration gradient. In contrast, we simulated the distribution of electrons in silicon when V_g = 30 V, as shown in Figure 4D. The vertical voltage causes the accumulation of induced carriers near the insulating layer and produces a decreasing concentration gradient when moving away from the bottom of top-silicon. This concentration gradient will generate a driving force for carrier diffusion and makes more photogenerated carriers diffuse into the heterojunction region, so the transport would be accelerated. Besides, the shortening of the falling time can be mainly ascribed to the enhanced concentration difference between the graphene and top-silicon regions under the positive voltage modulation, which leads to the acceleration of the carrier recombination. More experimental and modeling results about the response times are shown in Figure S6 of Supplementary Material, which clearly demonstrates the manipulation effect of voltage.

To further confirm the role of MPE, we have used heavily p-doped graphene as the device channel instead of the lightly doped ones. The corresponding transfer curve of the device can be seen in Figure S2(b) of the Supplementary Material, which demonstrates the graphene is heavily doped. Also, the relationship between I_{ds} and V_g in the dark state has been modeled to clarify the manipulation mechanism (see Figure S7 of the Supplementary Material). The manipulation effect of vertical voltage on the source-drain current under different optical power is shown in Figure 5A. The net photocurrent can be significantly changed under the manipulation of the vertical voltage. Obviously, as the optical power increases, the photocurrent will be enhanced. Note that the variation trend of I_{ds} is similar to the lightly p-doped GSOI device. The difference is that I_{ds} of the heavily p-doped GSOI device always keeps declining as V_g continuously increases because the type of the majority carriers doesn't change. Therefore, there is no "inflection point". Detailly speaking, the holes concentration of such graphene is extremely high, the conversion of majority carrier won't occur with the increase of V_g. The reliability of the mechanism was further verified by utilizing a moderately p-doped graphene device, as shown in Figure S2 of the Supplementary Material.

Figure 5B shows the I_{ds}-Time curve of the device when V_g = 0, −30 and 30 V. It can be seen that V_g not only enhances the photo response greatly but also leads to a negative net photocurrent. This effect can be attributed to the manipulation of top-silicon, which alters the relative position of the energy band between silicon and graphene,

Table 1: Summary of device parameters of several typical graphene photodetectors previously reported, and our device, including responsivity, response speed, and normalized detectivity.

Types of devices	Responsivity	Response speed	Normalized Detectivity
Graphene–metal junction [28]	6.1 mA/W	4 ps	–
Graphene–silicon heterojunction [41, 42]	0.435 A/W	160 μs	2.1×10^8 Jones
Graphene–silicon heterojunction in conductor mode [27]	10^4 A/W	60 μs	–
Graphene–silicon in QCR mode [23]	10^6–10^7 A/W	1.8 ms	7.69×10^9 Jones
Graphene-dioxide silicon /silicon [26]	10^3 A/W	400 ns	1.1×10^{10} Jones
Graphene–silicon-on-insulator [43]	0.23 A/W	20 ns	7.83×10^{10} Jones
Graphene-n-type silicon heterojunction [44]	0.73 A/W	750 μs	5.77×10^{13} Jones (calculated)
Our device: Graphene/silicon-on-insulator (GSOI) in conductor mode	10^7 A/W	90 μs	1.46×10^{13} Jones (measured) 1×10^{14} Jones (calculated)

and ultimately changes the direction of charge transport. Figure 5C shows the relationship of the responsivity with light power, in which the responsivity magnitude can increase by 5–10 times and reach the order of 10^6 A/W when $V_g = 30$ V, compared with the case without vertical voltage. The response time under different V_g is shown in Figure 5D, which exhibits an obvious decrease when V_g becomes positive or negative, and it can be as short as 90 μs. To strictly compare the GSOI photodetector with other reported devices, the detectivity was measured through the noise testing platform [38], the relevant formula is expressed as

$$D^* = \frac{\sqrt{\Delta f} \cdot A}{NEP} \tag{3}$$

where D^* is specific detectivity, A is device area and NEP is the noise equivalent power. The noise test method is described in detail in Figure S8 of Supplementary Material. Note that the measured detectivity is up to 1.46×10^{13} Jones. Alternatively, we can also directly calculate the detectivity by formula $D^* = \frac{A^{1/2}R}{(2qI_d)^{1/2}}$, where I_d is dark current and R is responsivity, as reported in other literature [39, 40]. The calculated detectivity of is up to 1×10^{14} Jones. Note that both the measured and calculated detectivities are much higher than other reported graphene-silicon hybrid devices, as shown in Table 1.

3 Conclusion

In this paper, a mechanism based on GSOI hybrid structure was proposed for the first time to obtain an adjustable built-in potential between graphene and silicon, which brings in an enhanced responsivity and fast response time. At the same time, due to the voltage manipulation, the concentration gradient of major carriers from the silicon to graphene is generated, which makes the photogenerated carriers diffuse rapidly to the depletion layer, thus the response time can be shortened. By manipulation, the responsivity can be increased from 10^5 to 10^7 A/W, and the response time is decreased from about 1000–90 μs for the GSOI device. The reliability of this manipulation mechanism is verified by a series of experiments and simulations with different doping types of graphene. The GSOI structure and manipulation mechanism in this paper pave the way to explore novel photodetectors with intriguing performance.

4 Methods

4.1 Device fabrication

For the photodetector fabrication, the SOI substrates were chosen, in which the thicknesses of top-silicon and bottom-silicon are 220 and 500 μm, respectively, and the thickness of the middle oxide layer is 2 μm. The primary specification parameter of the SOI can be seen in Section S9 of the Supplementary Material. The phosphorus doping concentrations for both silicon layers are 1×10^{15} cm^{-3}. To transfer graphene films onto the patterned substrates, the graphene-coated Cu foil was firstly spin-coated with polymethyl methacrylate (PMMA) and baked on a hot plate at 150 °C for 10 min. Subsequently, a mixed solution of hydrochloric acid and Hydrogen peroxide was used as an etchant, to remove the copper films. Lastly, the PMMA films were dissolved by using acetone after the accomplishment of the transfer process.

To make the electrodes, two kinds of photoresists, namely LOR and S1805, were successively spin-coated onto the graphene surface. After that, these photoresists were exposed and developed in AZ300 solution. Au film (50 nm) was sputtered onto the graphene surface by using e-beam evaporation, and will not directly contact with the top-silicon. Both the source and drain electrodes were obtained by dissolving the unexposed photoresists using the acetone solution.

To make the graphene film into strips, a second bilayer photolithography process was utilized. After the development, the uncovering graphene was etched by using oxygen for about 30 s. Lastly, the GSOI devices with the graphene strips of 10×10 μm) were obtained by dissolving the remaining photoresists in AZ400 solution.

4.2 Test characterization

The chip package was inserted into a socket located inside a home-built chamber connected to a Keithley semiconductor analyzer

(SCS4200) for electrical measurements under ambient conditions. Three probes were connected to SUM 1, SUM 2, and SUM three of SCS 4200. When measuring the manipulation curve, the source-drain bias was applied to 1 V, and the gate voltage was scanned from –60 to 60 V. The vertical voltage and source-drain bias remained unchanged when measuring the transient characteristics photoresponse. The response time was measured by a 7510-oscilloscope, which can guarantee the precise measurement of photoresponse with subtle magnitude.

4.3 Numerical simulation

The simulation model was solved by the finite element method based on a two-dimensional system. Simulations of the structures have been carried out by self-consistently solving the 2D electrostatic and transport equations. In particular, we solve

$$\begin{cases} J_n = qn\mu_n E + qD_n \nabla n \\ J_p = qp\mu_p E - qD_p \nabla p \end{cases}$$
$$\nabla \cdot \nabla\psi = -\frac{q}{\varepsilon}[p - n]$$

Among them, J_n and J_p are the current densities of electrons and holes, q is the single-electron charge, ε is the dielectric constant, n and p are the concentration of free electrons and holes. μ_n and μ_p denote the mobility of electrons and holes, $D_{n,}$ and D_p represent the diffusion coefficient of electrons and holes, respectively, and ψ is the potential. Assume that $D_{n,p}$ obeys the Einstein relation, namely $D_{n,p} = \mu_{n,p}\frac{k_B T}{q}$, where the thermal voltage $V_t = \frac{k_B T}{q}$, k_B is the Boltzmann constant and T is the absolute temperature, then the formula is changed to

$$\begin{cases} J_n = -qn\mu_n \nabla \psi + kT\mu_n n \\ J_p = -qp\mu_p \nabla \psi - kT\mu_p p \end{cases}$$

Because the device is in steady-state when it works stably, it can be considered that the concentration of electrons and holes does not change as the time varies. Thus, $\partial n/\partial t = 0$ and $\partial p/\partial t = 0$, which can be simplified to

$$\begin{cases} \dfrac{\partial n}{\partial t} = \dfrac{1}{q}\nabla \cdot J_n + U_n \\ \dfrac{\partial p}{\partial t} = -\dfrac{1}{q}\nabla \cdot J_p + U_p \end{cases}$$

$$\begin{cases} \nabla \cdot J_n = qU \\ \nabla \cdot J_p = -qU \end{cases}$$

U denotes the difference between net production rate G and compound rate R, thus $U = G - R(n, p)$. In the heavily doped devices, an SRH composite model was adopted, and the relevant formula is as follows:

$$R_{SRH} = \frac{np - n_i^2}{\tau_n(n + n_i^2) + \tau_p(p + p_i^2)}$$

Among them, $\tau_n(\tau_p)$ is electron (hole) lifetime, and n_i denotes the intrinsic carrier concentration.

The intensity attenuation of monochromatic light through semiconductor materials can be expressed as follows:

$$I = I_0 e^{-\alpha y}$$

where I_0 is the intensity of the incident light, and α is the absorption coefficient of the material. Generally, the absorption coefficient has a relationship with the wavelength. Given the relationship between photon absorption and electron-hole pair generation, carrier generation rate and light attenuation in semiconductors can be judged. Therefore, the light generation rate can be obtained as follows

$$G_L(y, \lambda) = G_{L0} e^{-\alpha y}$$

The G_{L0} in the above formula is the optical absorptivity on the semiconductor surface. For the reciprocal 1/α of the absorptivity, it is a dimension of length, representing the average penetration depth in the material.

When a light source is added to Silvaco TCAD to irradiate the semiconductor devices, the reflection and projection coefficients of each optical path, the loss caused by absorption and other factors will be accumulatively analyzed in the calculation. The following formulas will be used for light generation in materials:

$$G = \eta_0 \frac{P\lambda}{hc}\alpha e^{-\alpha y}$$

The physical quantities represented by the parameters in the formula are as follows: P is the intensity of the beam, which includes all factors affecting the reflection, transmission of the beam and attenuation due to the absorption in the propagation process; η_0 is the internal quantum efficiency, i.e. the number of electron holes produced by each incident photon; y is the relative distance of propagation in the solution process; h, c, and λ are Planck constants, light speed, and incident light wavelength, respectively; α is the absorption coefficient of the material.

Surface recombination is considered as a possible loss mechanism at the semiconductor interface, especially for bulk heterojunction materials with high mobility. Contact current is the equation of excess carrier concentration. That is to say, electron current density J_n^{cont} and hole current density J_p^{cont} include extraction, injection, and composite parts when contact:

$$J_n^{\text{cont}} = -qR_n^{\text{cont}} = -qS_n(n - n_{\text{eq}})$$
$$J_p^{\text{cont}} = -qR_p^{\text{cont}} = -qS_p(p - p_{\text{eq}})$$

The properties of the contact end depend on the surface recombination rate $S_{n,p}$ and the equilibrium concentration of free carriers n_{eq} and p_{eq}, which are related to the injection barrier $\phi_{n,p}$ of electrons and holes. The value of this parameter is affected by the quality of both materials and the presence of impurities.

Acknowledgments: This work was supported by the National Key R&D Program of China (2017YFE0131900), and Natural Science Foundation of Chongqing, China (cstc2019jcyjjqX0017).

References

[1] F. H. L. Koppens, T. Mueller, Ph. Avouris, A. C. Ferrari, M. S. Vitiello, and M. Polini, "Photodetectors based on graphene, other two-dimensional materials and hybrid systems," *Nat. Nanotechnol.*, vol. 9, pp. 780–793, 2014.

[2] P. Avouris and M. Freitag, "Graphene photonics, plasmonics, and optoelectronics," *IEEE J. Sel. Top. Quantum. Electron.*, vol. 20, 2014, Art no. 6000112.

[3] F. Bonaccorso, Z. Sun, T. Hasan, and A. C. Ferrari, "Graphene photonics and optoelectronics," *Nat. Photon.*, vol. 4, pp. 611–622, 2010.
[4] N. Guo, W. D. Hu, T. Jiang, et al., "High-quality infrared imaging with graphene photodetectors at room temperature," *Nanoscale.*, vol. 8, pp. 16065–16072, 2016.
[5] L. Tong, X. Y. Huang, P. Wang, et al., "Stable mid-infrared polarization imaging based on quasi-2D tellurium at room temperature," *Nat. Commun.*, vol. 11, p. 2308, 2020.
[6] Q. J. Liang, Q. X. Wang, Q. Zhang, et al., "High-performance, room temperature, ultra-broadband photodetectors based on air-stable PdSe2," *Adv. Mater.*, vol. 31, 2019, Art no. 1807609.
[7] R. R. Nair, P. Blake, A.N. Grigorenko, et al., "Fine structure constant defines visual transparency of graphene," *Science.*, vol. 320, pp. 1308–1308, 2008, https://doi.org/10.1126/science.1156965.
[8] M. Engel, M. Steiner, A. Lombardo, et al., "Light-Matter interaction in a microcavity-controlled graphene transistor," *Nat. Commun.*, vol. 3, p. 906, 2012.
[9] M. Furchi, A. Urich, A. Pospischil, et al., "Microcavity-Integrated graphene photodetector," *Nano. Lett.*, vol. 12, pp. 2773–2777, 2012.
[10] B. Zhao, J. M. Zhao, and Z. M. Zhang, "Enhancement of near-infrared absorption in graphene with metal gratings," *Appl. Phys. Lett.*, vol. 105, p. 031905, 2014.
[11] T. J. Echtermeyer, L. Britnell, P. K. Jasnos, et al., "Strong plasmonic enhancement of photovoltage in graphene," *Nat. Commun.*, vol. 2, p. 458, 2011.
[12] Z. Y. Fang, Y. M. Wang, Z. Liu, et al., "Plasmon-Induced doping of graphene," *Acs. Nanotechnol.*, vol. 6, pp. 10222–10228, 2012.
[13] H. H. Fang and W. D. Hu, "Photogating in low dimensional photodetectors," *Adv. Sci.*, vol. 4, p. 1700323, 2017.
[14] G. Konstantatos, M. Badioli, L. Gaudreau, et al., "Hybrid graphene-quantum dot photo transistors with ultrahigh gain," *Nat Nanotechnol.*, vol. 7, pp. 363–368, 2012.
[15] Z. H. Sun, Z. K. Liu, J. H. Li, G. A. Tai, S. P. Lau, and F. Yan, "Infrared photodetectors based on CVD-grown graphene and Pbs quantum dots with ultrahigh responsivity," *Adv. Mater.*, vol. 24, pp. 5878–5883, 2012.
[16] Y. Lee, J. Kwon, E. Hwang, et al., "High-performance perovskite-graphene hybrid photodetector," *Adv. Mater.*, vol. 27, pp. 41–46, 2015.
[17] Y. Liu, F. Wang, X. Wang, et al., "Planar carbon nanotube-graphene hybrid films for high-performance broadband photodetectors," *Nat. Commun.*, vol. 6, p. 8589, 2015.
[18] K. Roy, M. Padmanabhan, S. Goswami, et al., "Graphene–MoS_2 hybrid structures for multifunctional photoresponsive memory devices," *Nat. Nanotechnol.*, vol. 8, pp. 826–830, 2013.
[19] F. H. L. Koppens, T. Mueller, P. Avouris, A. C. Ferrari, M. S. Vitiello, and M. Polini, "Photodetectors based on graphene, other two-dimensional materials and hybrid systems," *Nat. Nanotechnol.*, vol. 9, pp. 780–793, 2014.
[20] Q. S. Guo, A. Pospischil, M. Bhuiyan, et al., "Black phosphorus mid-infrared photodetectors with high gain," *Nano. Lett.*, vol. 16, p. 4648, 2016.
[21] C. Soci, A. Zhang, B. Xiang, et al., "ZnO nanowire UV photodetectors with high internal gain," *nanosci. Nanotechnol.*, vol. 10, p. 1430, 2010.
[22] G. Konstantatos, M. Badioli, L. Gaudreau, et al., "Graphene–Quantum dot phototransistors with ultrahigh gain," *Nat. Nanotechnol.*, vol. 7, pp. 363–368, 2012.
[23] F. Z. Liu and S. Kar, "Quantum carrier reinvestment-induced ultrahigh and broadband photocurrent responses in graphene-silicon junctions," *Acs. Nano.*, vol. 8, pp. 10270–10279, 2014.
[24] I. Nikitskiy, S. Goossens, D. Kufer, et al., "Integrating an electrically active colloidal quantum dot photodiode with a graphene phototransistor," *Nat. Commun.*, vol. 7, 2016, Art no. 11954
[25] B. Radisavljevic and A. Kis, "Mobility engineering and a metal-insulator transition in monolayer MoS2," *Nat. Mater.*, vol. 12, pp. 815–820, 2013.
[26] X. T. Guo, W. H. Wang, H. Nan, et al., "High-performance graphene photodetector using interfacial gating," *Optica.*, vol. 3, pp. 1066–1070, 2016.
[27] Z. F. Chen, Z. Z. Cheng, J. Q. Wang, et al., "High responsivity, broadband, and fast graphene/silicon photodetector in photoconductor mode," *Adv. Opt. Mat.*, vol. 3, pp. 1207–1214, 2015.
[28] F. Xia, T. Mueller,Y.-M. Lin, A. Valdes-Garcia, and P. Avouris, "Ultrafast graphene photodetector," *Nat. Nanotechnol.*, vol. 4, pp. 839–843, 2009.
[29] Y. Liu, R. Cheng, L. Liao, et al., "Plasmon resonance enhanced multicolour photodetection by graphene," *Nat. Commun.*, vol. 2, p. 579, 2011.
[30] J. J. Liu, Y. L. Yin, L. H. Yu, Y. Shi, D. Liang, and D. Dai, "Silicon–Graphene conductive photodetector with ultra-high responsivity," *Sci. Reports.*, vol. 7, 2017, Art no. 40904.
[31] S. Riazimehr, S. Kataria, J. M. Gonzalez-Medina, et al., "High responsivity and quantum efficiency of graphene/silicon photodiodes achieved by interdigitating Schottky and gated regions," *Acs Photon.*, vol. 6, pp. 107–115, 2019.
[32] K. S. Novoselov, A. K. Geim, S. V. Morozov, et al., "Electric field effect in atomically thin carbon films," *Science.*, vol. 306, pp. 666–669, 2004.
[33] D. Reddy, L. F. Register, G. D. Carpenter, and S. K. Banerjee, "Graphene field-effect transistors," *J. Phy. D-Appl. Phy.*, vol. 45, 2012, Art no. 019501.
[34] M. S. Mobarakeh, N. Moezi, M. Vali, and D. Dideban, "A novel graphene tunnelling field effect transistor (GTFET) using bandgap engineering," *Superlatt. Microstruct.*, vol. 100, pp. 1221–1229, 2016.
[35] A. Safari, M. Dousti, and M. B. Tavakoli, "Monolayer graphene field effect transistor-based operational amplifier," *J. Circuits Sys. Comp.*, vol. 28, 2019, Art no. 1950052.
[36] K. Chen, X. Wan, D. Q. Liu, et al., "Quantitative determination of scattering mechanism in large-area graphene on conventional and SAM-functionalized substrates at room temperature," *Nanoscale.*, vol. 5, p. 5784, 2013.
[37] X. S. Li, C. W. Magnuson, A. Venugopal, et al., "Large-area graphene single crystals grown by low-pressure chemical vapor deposition of methane on copper," *Am. Chem. Soc.*, vol. 133, p. 2816, 2011.
[38] Y. J. Fang, A. Armin, P. Meredith, and J. S. Huang, "Accurate characterization of next-generation thin-film photodetectors," *Nat. photon.*, vol. 13, pp. 1–4, 2019.

[39] K. E. Chang, C. Kim, T. J. Yoo, et al., "High-responsivity near-infrared photodetector using gate-modulated graphene/germanium Schottky junction," *Adv. Electronic Mater.*, vol. 5, 2019, Art no. 1800957.
[40] J. Shen, X. Z. Liu, X. F. Song, et al., "High-performance Schottky heterojunction photodetector with directly grown graphene nanowalls as electrodes," *Nanoscale.*, vol. 9, pp. 6020–6025, 2017.
[41] X. An, F. Liu, Y. J. Jung, and S. Kar, "Tunable graphene-silicon heterojunctions for ultrasensitive photodetection," *Nano. Lett.*, vol. 13, pp. 909–916, 2013.
[42] Y. B. An, A. Behnam, E. Pop, and A. Ural, "Metal-semiconductor-metal photodetectors based on graphene/p-type silicon Schottky junctions," *Appl. Phys. Lett.*, vol. 102, 2013, Art no. 013110.
[43] H. Selvi, E. W. Hill, P. Parkinson, and T. J. Echtermeyer, "Graphene-silicon-on-insulator (GSOI) Schottky diode photodetectors," *Nanoscale.*, vol. 10, pp. 18926–18935, 2018.
[44] X. M. Li, M. Zhu, M. D. Du, et al., "High detectivity graphene-silicon heterojunction photodetector," *Small.*, vol. 12, pp. 595–601, 2016.

Supplementary Material: The online version of this article offers supplementary material (https://doi.org/10.1515/nanoph-2020-0261).